Direct chemical discrimination at step edges and kink sites of sodium chloride by nc-AFM with an oxygen-terminated copper tip

Philipp Wiesener [1], Saeed Amirjalayer [2,*] and Harry Mönig [1,†]

[1] *Physical Institute, University of Münster, Wilhelm-Klemm-Straße 10, Münster 48149, Germany*

[2] *Interdisciplinary Center for Scientific Computing, University of Heidelberg, Berliner Straße 43, Heidelberg 69120, Germany*

(Received 9 September 2025; accepted 4 March 2026; published 19 March 2026)

Since the advent of scanning probe microscopy, elemental- and chemical discrimination on heterogeneous surfaces has been a major challenge. This is mainly due to complex contrast mechanisms, which require considerable indirect structural assumptions of tip and surface and related extensive theoretical modeling. Previously, noncontact atomic force microscopy with atomically defined copper oxide tips (CuOx-tips) showed elemental selectivity on even most complex metal-oxide surfaces [Hütner *et al.*, Science **385**, 1241, 2024]. Here we report an investigation of an ionic surface, which allows to directly identify the anionic- and cationic sub lattices even on aperiodic surface structures. In line with previous work on metal oxides [Wiesener *et al.*, ACS Nano **18**, 21948, 2024], the present results extend chemically selective imaging of CuOx-tips to a new class of heterogeneous materials.

DOI: 10.1103/297b-7fpm

I. INTRODUCTION

In scanning probe microscopy, the identity and bonding configuration of the terminal atom at the probe-tip drastically affects the image contrast [1–3]. Especially in the field of noncontact atomic force microscopy (nc-AFM) in conjunction with the qPlus sensor technique [4], tremendous progress has been made by implementing a variety of tip-functionalization approaches. These include tips with halogen, or Xe-terminations [1,5–7], or hydrogen-terminated tips [8], or tips terminated with single molecules [9–12], all of which show differences in charge distribution, reactivity, and mechanical flexibility [3,13]. By far the most common approach is to attach a single CO molecule to a metallic tip. This chemically passivates the apex and facilitates imaging in the repulsive force regime where nanostructures can be imaged with submolecular and even subatomic contrast. In fact, the combination of the qPlus sensor and CO-tip led to outstanding progress and a new era in surface chemistry [4,14–16].

In recent years, oxygen-terminated copper tips (CuOx-tips) have been established as a promising further alternative in atomic-scale tip-functionalization. Besides a partial chemical passivation within the tip-sample junction, CuOx-tips stand out with an exceptional rigidity, which not only allows imaging with submolecular resolution, but also significantly reduced artifacts due to tip flexibility [3,17,18]. Furthermore, systematic CuOx-tip nc-AFM experiments on a variety of different metal-oxide surfaces showed a distinct elemental sensitivity, which provides immediate access to the metal- and oxygen sublattices of even the most complex surfaces [19–22]. The pronounced nc-AFM contrast of metal- and oxygen sites can largely be explained by electrostatic considerations. The oxygen atom terminating a CuOx-tip accumulates negative charge at the apex, which can be quantified by a Bader charge analysis of an optimized tip structure to about $-1e$ [17]. As a consequence of this tip charge and the high rigidity of CuOx-tips, constant-height imaging of a metal-oxide surface leads to a distinct repulsive interaction above surface oxygen sites, whereas on metal sites attractive interactions dominate. Therefore, the strongly varying potential of metal-oxide surfaces is directly reflected in the corresponding nc-AFM contrast where negative oxygen sites appear bright and positive metal sites as depressions with excellent qualitative agreement between experimental and simulated data [22].

In the present study, we investigate if the clear elemental selectivity observed on metal-oxide surfaces also applies for ionic materials. As a model system we chose sodium chloride, which is grown as bi- and trilayers on Cu(111). Its basic structure and well-established properties facilitates the understanding of nc-AFM or Kelvin probe force microscopy (KPFM) contrasts [23–25], which is of high relevance for the elucidation of more complex heterogeneous surface structures [26–29]. In a first step we investigate the contrast on a flat NaCl(100) terrace, which is discussed with accompanying electrostatic potential simulations based on density functional theory (DFT). In a second step, aperiodic sites in the form of a linear and a kinked step edge are investigated, to analyze how the contrast depends on the local chemical environment of a specific atom. The qualitative agreement between experimental data and simulated electrostatic potential maps suggests that the contrast in the attractive force regime is indeed largely determined by the interaction of the negative charge at the

*Contact author: saeed.amirjalayer@iwr.uni-heidelberg.de

†Contact author: harry.moenig@uni-muenster.de

Published by the American Physical Society under the terms of the Creative Commons Attribution 4.0 International license. Further distribution of this work must maintain attribution to the author(s) and the published article's title, journal citation, and DOI.

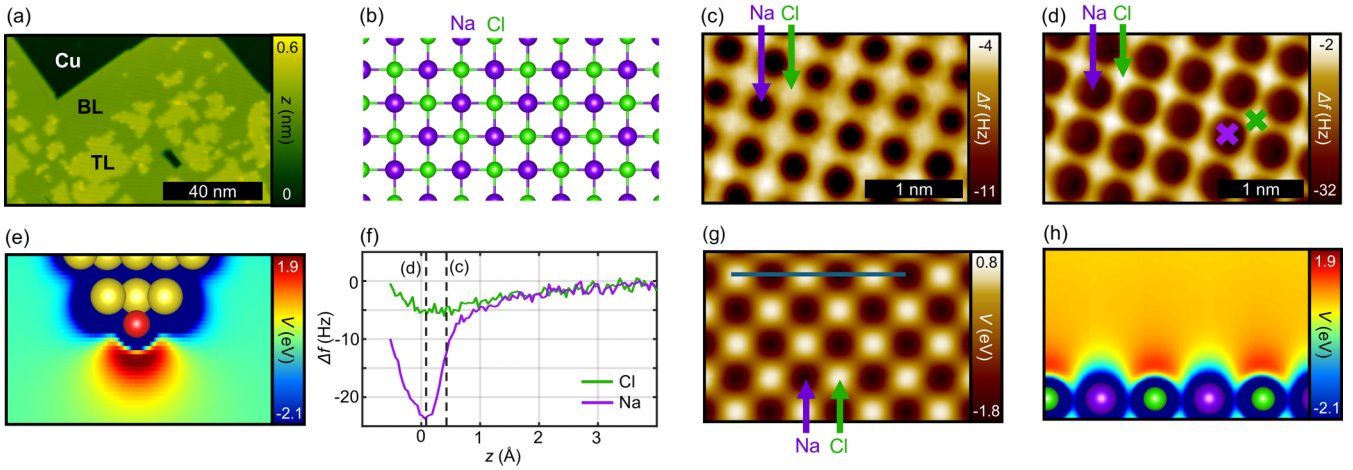


FIG. 1. Flat NaCl terrace. (a) Overview STM image of bi-layerd (BL) and tri-layerd (TL) NaCl-islands on Cu(111) (feedback 10 pA, 2V). (b) Top view of DFT-optimized surface. (c), (d) CuOx-tip constant height nc-AFM recorded on a flat NaCl-terrace in the attractive force regime with two different tip-sample distances (d) is recorded about 40 pm closer. (e) Cross section of the calculated electrostatic potential of the CuOx-tip. (f) $\Delta f(z)$ spectra on the sites marked in (d). $z = 0$ corresponds to the tip height of the measurement in (d). The dashed lines correspond to the heights, where the measurements were recorded. (g) Calculated electrostatic potential of the NaCl-surface shown in (b), plotted at a height of 166 pm relative to the top most surface atom. This height is consistent with the results previously obtained for metal oxides [22]. (h) Cross section of the calculated electrostatic potential of the NaCl surface along the blue line in (g).

tip apex and the anionic/cationic surface atoms. Consistent with previous work on metal oxides [22], these results extend chemically selective imaging and qualitative electrostatic potential mapping with CuOx tips to ionic surfaces, broadening their applicability to a new class of heterogeneous materials.

II. METHODS

The experiments were performed with a qPlus force sensor allowing nc-AFM and scanning tunneling microscopy (STM) [4], operated under ultra-high vacuum and liquid nitrogen temperature (78 K). For DFT simulations, the Vienna *Ab Initio* Simulation Package (VASP) was used [30,31]. Atomistic investigations were conducted on the NaCl surfaces focusing on the electrostatic potential $V(r)$ calculated as

$$V(r) = V_{\text{ionic}}(r) + \int \frac{n(r')}{|r - r'|} dr'$$

with the electron density $n(r)$, the ionic potential $V_{\text{ionic}}(r)$, and the Hartree potential of the surfaces. More details on experimental- and the theoretical methods are provided as Supplemental Material [32].

III. RESULTS AND DISCUSSION

A. Contrast on flat terraces

Depositing NaCl by thermal evaporation on metal surfaces leads to the growth of (100)-terminated bi- or tri-layered crystalline islands [33,34]. Figure 1(a) shows an STM overview image of such NaCl-layers grown on Cu(111), while Fig. 1(b) illustrates the DFT-optimized NaCl(100) surface. The alternating anionic and cationic surface species contribute to a nearly planar surface layer, where the Cl ions protrude only about 12 pm above the Na ions. Figures 1(c) and 1(d) show CuOx-tip nc-AFM measurements recorded in constant-height mode at two different heights within the attractive force regime revealing a pronounced contrast reflecting the 1x1 geometry. The CuOx-tip is negatively terminated [Fig. 1(e)] and its contrast is mainly described by electrostatics in this regime. Therefore, the tip shows pronounced attraction to the positive Na ions whereas the interaction with the negative Cl ions is more repulsive. This elemental selectivity is further reflected in $\Delta f(z)$ spectra recorded on the different sites [Fig. 1(f)], where a distinct separation of the curves over an extended height-range can be observed. Particularly, the strongest elemental contrast is achieved at a tip-height z around the $\Delta f(z)$-minimum on the Na-site, where the difference between both $\Delta f(z)$ curves is maximized. Since the Na and Cl ions are nearly co-planar, the observed contrast can be directly related to a distinct elemental selectivity achieved with the CuOx-tip for this ionic surface. The electrostatic potential calculated from the DFT-optimized structure shown in Fig. 1(g), shows excellent agreement with the observed experimental contrast and underpins that the elemental selectivity is largely dominated by electrostatic tip-sample interactions. This is further supported by corresponding CuOx-tip AFM simulations, both with and without the electrostatic contribution (Fig. S2 [32]), demonstrating that a significant elemental contrast is achieved only when electrostatics are included. In nc-AFM, the surface potentials are inherently entangled with the measured force interactions, limiting the described contrasts to a qualitative assessment of the electrostatic potential. To achieve also quantitative information about the electrostatic potential, complementary techniques such as 3D-AFM, KPFM [35] or scanning quantum dot microscopy [36,37] could be used, all of which have achieved remarkable progress in mapping the electrostatic potential of surfaces even quantitatively.

In our work, the electrostatic potential is plotted at a height of 166 pm relative to the top most surface atom, as within this height regime the most consistent and best qualitative agreement with the experiment is found [22]. Certainly, this height cannot be directly translated to an absolute tip-sample

distance for the experiment. For this we consider the overlap of the electrostatic potentials of both the surface and the tip within the tip-sample junction (Figs. 1(e) and 1(h), see further illustration in Fig. S1 [32]). Assuming a similar distance for the electrostatic potential maximum [red area in Fig. 1(e)] of the tip of about 166 pm, a rough estimation results in a tip-sample distance of 320 pm ± 20 pm between the oxygen atom of the tip and surface atoms. Please note, that this result is consistent with the DFT-derived force-distance curves reported by Schulze Lammers *et al.* [3]. A cross section of the electrostatic potential along the blue line in Fig. 1(g) is represented in Fig. 1(h), further illustrating the heterogeneous charge distribution above the surface layer induced by the negative Cl and positive Na ions. These results show that the elemental nc-AFM contrast of CuOx-tips, previously found for metal oxide surfaces [22], also applies to ionic surfaces.

B. Analysis of NaCl step edges

In addition to the nc-AFM contrast for the flat terraces, aperiodic surface sites, e.g., step edges and kinks of the NaCl islands are analyzed. The DFT-optimized structure of a NaCl step edge between a bi- and trilayer is shown in Fig. 2(a). To maintain charge neutrality, step edges always form along the [100] or [010] directions, preventing the formation of exclusively Na- or Cl-terminated step-edges [33,34]. A large-scale constant-height nc-AFM image acquired with a CuOx-tip around an area of a NaCl step edge is presented in Fig. 2(b). The nc-AFM contrast along the step edge differs significantly from the contrast observed on the flat terraces. In addition, a much more pronounced contrast is observed at the island kink (red arrow), which will be addressed in the following section. Sodium and chloride ions at the step edges exhibit a lower coordination compared to those in the terrace. Bennewitz *et al.* [38] have previously elucidated the resulting AFM contrast, attributing it to two main factors: First, due to their reduced coordination and weaker binding with neighboring ions, the step-edge ions protrude by several picometers Δz (20–30 pm), as an effect of the AFM tip [illustrated in Fig. 2(c)]. Second, the lower coordination alters the electrostatic potential along the edge, which in turn affects the AFM contrast.

To elucidate the observed contrast at the step edge, we calculated the corresponding lateral and vertical plots of the electrostatic potential for the DFT-optimized structure in Figs. 2(d) and 2(e) as well as a corresponding CuOx-tip AFM simulation in Fig. S2 [32], which align well with the observed experimental contrast. Compared to the flat terraces, the step-edge ions associated potentials are laterally more extended [Figs. 2(d)–2(f)]. However, the absolute value of the electrostatic potential within the plane of imaging of a Na step ion differs not much from the Na terrace species [Fig. 2(f)]. A high resolution constant-height nc-AFM image using a CuOx-tip with reduced tip-sample distance along a NaCl step edge is shown in Fig. 2(g). The measurement reveals that the overall tip-sample interaction is dominated by the positive Na ions, rather than by the negative Cl ions. Due to the negatively terminated CuOx-tip, the stronger electrostatic attraction to the positive Na step-edge ions leads to a more pronounced elevation compared to the negative Cl ions [38]. Consequently, a distinct topographic height of Na and Cl ions at the step edge can be expected, leading to the observed contrast. Additionally, the round shaped region of attractive tip-sample interaction of these step-edge Na ions is spatially extended compared to the terrace ions due to the electrostatic potential laterally spreading from the step edge. It should be noted that the contrast observed with a CuOx-tip differs from the contrast reported previously for CO-tip measurements [24,39]. This difference can be attributed to the stronger sensitivity of the CuOx-tip to electrostatic tip-sample interactions and the absence of tip-bending artifacts, as discussed extensively in previous studies [3,13]. Simultaneously, the Na ions contrast at the step edge show a distinct bright center reflecting emerging repulsive forces, which is attributed to their elevation caused by the tip. This vertical displacement of Na ions is further

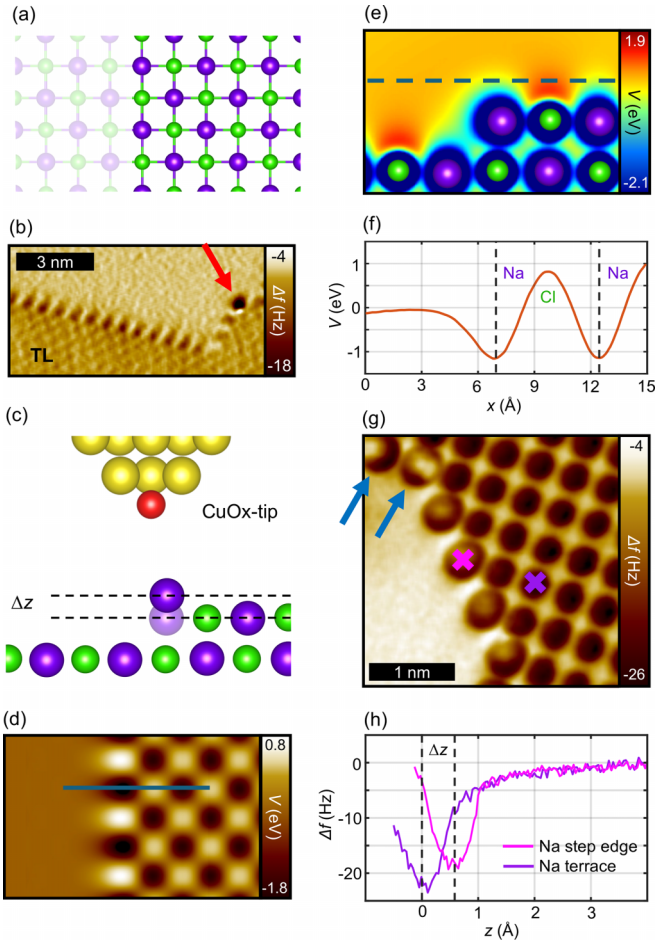


FIG. 2. NaCl step edge. (a) DFT-optimized structure as top view. (b) CuOx-tip constant height nc-AFM. (c) Illustration of the protruding step edge ion by Δz as an effect of the AFM tip. (d) Electrostatic potential of the NaCl step edge shown in (a), plotted at a height of 166 pm relative to the top most surface atom. (e) Cross section of the electrostatic potential along the blue line in (d). (f) Line-profile extracted along the dashed line in (e) at a height of 166 pm relative to the top most surface atom. (g) High-resolution CuOx-tip constant height nc-AFM. The blue arrow marks the Na re-entrant kink sites where the step edge changes direction. (h) $\Delta f(z)$ spectra of the Na sites marked in g. $z = 0$ corresponds to the tip-height in (g).

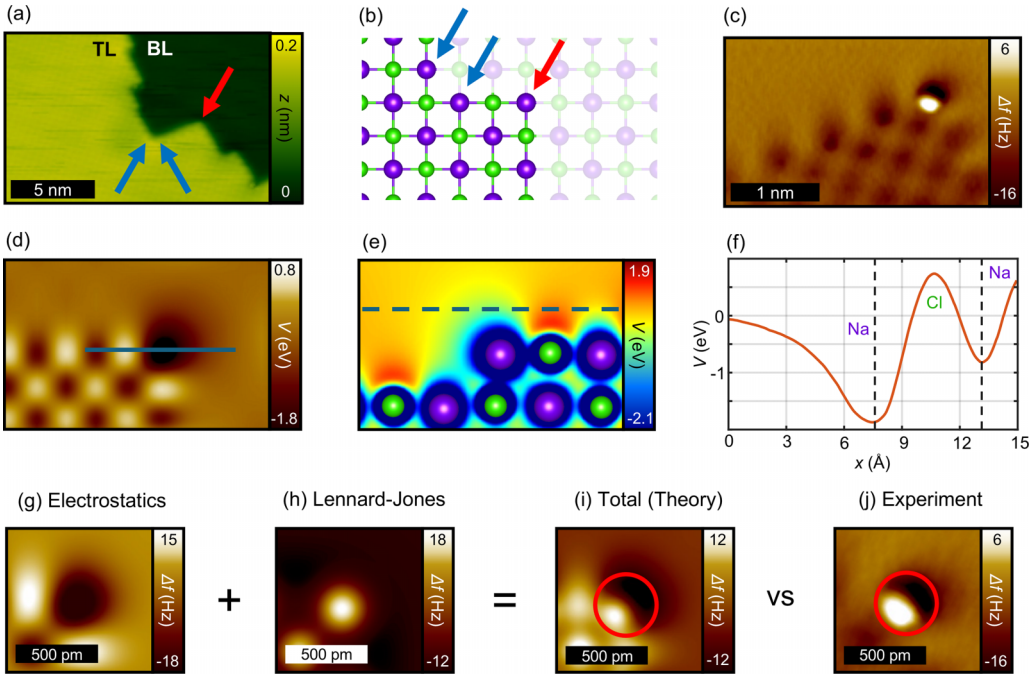


FIG. 3. Na kink. (a) Overview STM image (feedback 10 pA, 2V) and (b) structure of a re-entrant (blue arrow) and corner (red arrow) Na ion. (c) CuOx-tip nc-AFM of a Na corner ion. (d) Calculated electrostatic potential of a Na corner ion, plotted at a height of 166 pm relative to the top most surface atom. (e) Cross section of the calculated electrostatic potential along the blue line in (d). (f) Line-profile extracted along the dashed line in (e). (g)–(i) Probe-particle AFM simulation for a reduced tip-sample distance (decreased by 50 pm relative to the simulations in the attractive force regime shown in Fig. S2 [32]) calculated based on the electrostatic force (g), Lennard-Jones force (h), total force (i). The position of the Na corner ion according to the DFT structure is marked by the center of the red circle with a radius of 200 pm. (j) Corresponding experimental AFM.

emphasized in Fig. 2(h), which presents $\Delta f(z)$ spectra recorded over both Na surface species. The $\Delta f(z)$ minimum of the Na step edge site is shifted by (50 ± 5) pm compared to the terrace site. In contrast, simulated $\Delta f(z)$ spectra (Fig. S2 [32]) of the planar step-edge structure, in which no tip-induced ion elevation is included, do not exhibit such a shift. Consequently, as these spectra include the electrostatic tip-sample interaction of surrounding ions, the experimentally observed displacement of the $\Delta f(z)$ minimum can therefore fully be attributed to an elevation of the step-edge Na ions induced by the tip.

According to the DFT structure in Fig. 2(a), the Na ions along the step edge are separated by Cl ions exhibiting a relatively large Na-Na distance of 5.25 Å. However, this changes when considering the Na re-entrant kink sites where the step edge changes direction from the [100] to the [010] direction as marked by the blue arrows in Fig. 2(g) [see also Figs. 3(a) and 3(b)]. These Na step-edge ions exhibit both, a reduced coordination compared to the Na-terrace ions and a relatively small Na-Na distance of 3.62 Å without a Cl-ion in between. It is interesting to note the corresponding asymmetric appearance of these Na ions within the constant-height nc-AFM measurement. In contrast to the previously discussed step-edge sites, a pronounced repulsive contrast is revealed, which is eccentric offset to the attractive tip-sample interaction around the Na kink ions (blue arrows). Furthermore, the repulsive contrast of both Na kink ions is mirrored along the bisector of the re-entrant. In nc-AFM, asymmetries in contrast are typically attributed to tip asymmetries and corresponding imaging artifacts. However, the fact that the three neighboring step edge atoms in the top left of Fig. 2(g) show an repulsive contrast unevenly directed renders a tip-induced imaging artifact unlikely. Additionally, tip-induced asymmetries in the contrast are corrected during the tip-forming process [3]. At the same time, the observed AFM contrast of the kink sites is not reflected by the shown electrostatic potential, since the elevation Δz of the lower coordinated Na ions is leading to a significantly reduced local tip-sample distance and corresponding short-range force interactions with an increased repulsive component. A detailed theoretical analysis of the described contrast is beyond the scope of this manuscript. However, a more simplified approach of understanding the observed repulsive contrast is given by a similar measurement of a Na corner kink, which is shown in Figs. 3(a) and 3(b) marked with a red arrow.

C. Na terminated kinks

Sodium ions located at the corner of an island (theoretical binding energy of 4.0 eV) exhibit an coordination even lower than the step-edge ions (theoretical binding energy of 4.5 eV) discussed above. Therefore, the elevation and attraction to the AFM tip is drastically increased, which makes imaging these surface species extremely challenging. Approaching too close to the surface may result in the tip picking up the corner ion, thereby compromising the defined termination of the tip. However, an isolated Na corner ion could be imaged, which is shown in Fig. 3(c) [see also red arrow in Fig. 2(b)]. The corner ion appears significantly more attractive than adjacent

Na ions along the step edge and within the terrace, attributable to the altered electrostatic potential, depicted in Fig. 3(d) and as a cross section along the blue line in Figs. 3(e) and 3(f) (see also Fig. S2 for corresponding AFM simulations [32]). In the theoretical calculations, the Na corner ion appears more electropositive in both lateral extent and absolute intensity compared to neighboring step-edge ions as shown in the extracted line profile in Fig. 3(f).

Again, the nc-AFM measurement reveals a pronounced repulsive contrast, which is eccentric offset to the attractive tip-sample interaction around the Na corner ion. To disentangle the contributions of electrostatic- and emerging repulsive short-range forces to this contrast, a CuOx-tip probe particle AFM simulation [40] (see also Supplemental Material [32]) of the individual tip-sample interactions is shown in Figs. 3(g)–3(i). To account for the locally reduced tip-sample distance due to the tip-induced elevation of the Na ion at the kink site, the tip-sample distance is decreased by 50 pm relative to the simulations in the attractive force regime shown in Fig. S2 [32]. Firstly, the electrostatic tip-sample interaction (g) produces the attractive contrast (up to −18 Hz) due to the negative tip termination of the CuOx-tip and the shown electrostatic potential of the surface, as discussed above for the flat terraces and step edges. Secondly, the Lennard-Jones interaction (h), including Pauli repulsion, must also be considered due to the locally reduced tip-sample distance caused by the elevation and the corresponding overlap of charge densities between the tip and corner ion. As shown by the simulation, it mainly contributes to a repulsive contrast feature (up to +18 Hz) unlike the attractive electrostatics. The van der Waals attraction as part of the Lennard-Jones interaction, which primarily interacts with the bulk tip body, makes the smallest contribution (up to ±1 Hz). Experimentally, the measured tip-sample interaction is a superposition of all force interactions, summed in a simulation of the total force in Fig. 3(i). Here, the experimentally observed CuOx-tip nc-AFM contrast [Fig. 3(j)] for the single Na corner ion is well reproduced as the strong electrostatic interaction is superposed by emerging Pauli repulsion. In contrast to the Pauli repulsion, which follows the total electron density of the ion, the electrostatic potential also includes the ionic potential V_{ionic} of the core. According to our data, both quantities contribute to the observed asymmetric contrast at the kink ion. The electrostatic potential spread from the kink site and corresponding attraction is lateral, more extent compared to the electron densities sensed by Pauli repulsion. A fundamental aspect in describing the observed AFM contrast is the high rigidity of the CuOx-tip, preventing tip-flexibility artifacts, as well as the tip's terminating O atom, which accumulates negative charge at the tip apex rendering it as an idealized point charge probe.

IV. CONCLUSIONS

This study employs high-resolution qPlus nc-AFM of flat terraces, step edges, and kinks of NaCl, grown on Cu(111). The CuOx-tip functionalization enables elemental discrimination on terraces as well as at step edges and reveals differences in the electronic structure and coordination on a single-ion level. The underlying contrast mechanism is based on the CuOx-tip's high sensitivity to electrostatic tip-sample interactions, which enable the electrostatic potential of a surface to be qualitatively mapped. Furthermore, when imaging at a reduced tip-sample distance, the strong electrostatic sensitivity is superposed by emerging Pauli repulsion, while tip-bending artifacts can be largely neglected due to the high rigidity of the CuOx-tip. Our data allow us to conclude that the chemically selective nc-AFM contrast of CuOx-tips, previously found for metal oxide surfaces [22], also applies for ionic materials, and might even be generalized for other heterogeneous surface systems.

ACKNOWLEDGMENT

This work was funded by the Deutsche Forschungsgemeinschaft (DFG, German Research Foundation) through Project No. 527214857.

DATA AVAILABILITY

The data that support the findings of this article are not publicly available. The data are available from the authors upon reasonable request.

[1] L. Gross, F. Mohn, N. Moll, P. Liljeroth, and G. Meyer, The chemical structure of a molecule resolved by atomic force microscopy, Science **325**, 1110 (2009).

[2] T. Hofmann, F. Pielmeier, and F. J. Giessibl, Chemical and crystallographic characterization of the tip apex in scanning probe microscopy, Phys. Rev. Lett. **112**, 066101 (2014).

[3] B. Schulze Lammers, D. Yesilpinar, A. Timmer, Z. Hu, W. Ji, S. Amirjalayer, H. Fuchs, and H. Mönig, Benchmarking atomically defined AFM tips for chemical-selective imaging, Nanoscale **13**, 13617 (2021).

[4] F. J. Giessibl, The qPlus sensor, a powerful core for the atomic force microscope, Rev. Sci. Instrum. **90**, 011101 (2019).

[5] N. Pavliček, B. Schuler, S. Collazos, N. Moll, D. Pérez, E. Guitián, G. Meyer, D. Peña, and L. Gross, On-surface generation and imaging of arynes by atomic force microscopy, Nat. Chem. **7**, 623 (2015).

[6] P. Hapala, M. Švec, O. Stetsovych, N. J. Van Der Heijden, M. Ondráček, J. Van Der Lit, P. Mutombo, I. Swart, and P. Jelínek, Mapping the electrostatic force field of single molecules from high-resolution scanning probe images, Nat. Commun. **7**, 11560 (2016).

[7] J. N. Ladenthin, T. Frederiksen, M. Persson, J. C. Sharp, S. Gawinkowski, J. Waluk, and T. Kumagai, Force-induced tautomerization in a single molecule, Nat. Chem. **8**, 935 (2016).

[8] H. Labidi, M. Koleini, T. Huff, M. Salomons, M. Cloutier, J. Pitters, and R. A. Wolkow, Indications of chemical bond contrast in AFM images of a hydrogen-terminated silicon surface, Nat. Commun. **8**, 14222 (2017).

[9] F. Mohn, B. Schuler, L. Gross, and G. Meyer, Different tips for high-resolution atomic force microscopy and scanning tunneling microcopy of single molecules, Appl. Phys. Lett. **102**, 073109 (2013).

[10] G. Kichin, C. Weiss, C. Wagner, F. S. Tautz, and R. Temirov, Single molecule and single atom sensors for atomic resolution imaging of chemically complex surfaces, J. Am. Chem. Soc. **133**, 16847 (2011).

[11] A. M. Sweetman, S. P. Jarvis, H. Sang, I. Lekkas, P. Rahe, Y. Wang, J. Wang, N. Champness, L. Kantorovich, and P. Moriarty, Mapping the force field of a hydrogen-bonded assembly, Nat. Commun. **5**, 3931 (2014).

[12] T. Chutora, B. De La Torre, P. Mutombo, J. Hellerstedt, J. Kopecek, P. Jelinek, and M. Svec, Nitrous oxide as an effective AFM tip functionalization: A comparative study, Beilstein J. Nanotechnol. **10**, 315 (2019).

[13] D. Yesilpinar, B. Schulze Lammers, A. Timmer, Z. Hu, W. Ji, S. Amirjalayer, H. Fuchs, and H. Mönig, Mechanical and chemical interactions in atomically defined contacts, Small **17**, 2101637 (2021).

[14] F. Huber, J. Berwanger, S. Polesya, S. Mankovsky, H. Ebert, and F. J. Giessibl, Chemical bond formation showing a transition from physisorption to chemisorption, Science **366**, 235 (2019).

[15] M. Emmrich, F. Huber, F. Pielmeier, J. Welker, T. Hofmann, M. Schneiderbauer, D. Meuer, S. Polesya, S. Mankovsky, D. Ködderitzsch, H. Ebert, and F. J. Giessibl, Subatomic resolution force microscopy reveals internal structure and adsorption sites of small iron clusters, Science **348**, 308 (2015).

[16] L. Gross, B. Schuler, N. Pavliček, S. Fatayer, Z. Majzik, N. Moll, D. Peña, and G. Meyer, Atomic force microscopy for molecular structure elucidation, Angew. Chem. Int. Ed. **57**, 3888 (2018).

[17] H. Mönig, S. Amirjalayer, A. Timmer, Z. Hu, O. Liu, L. D. Arado, M. Cnudde, C. A. Strassert, W. Ji, M. Rohlfing, and H. Fuchs, Quantitative assessment of intermolecular interactions by atomic force microscopy imaging using copper oxide tips, Nat. Nanotechnol. **13**, 371 (2018).

[18] H. Mönig, Copper-oxide tip functionalization for submolecular atomic force microscopy, Chem. Commun. **54**, 9874 (2018).

[19] J. I. Hütner, A. Conti, D. Kugler, F. Mittendorfer, G. Kresse, M. Schmid, U. Diebold, and J. Balajka, Stoichiometric reconstruction of the Al_2O_3(0001) surface, Science **385**, 1241 (2024).

[20] G. Franceschi, A. Conti, L. Lezuo, R. Abart, F. Mittendorfer, M. Schmid, and U. Diebold, How water binds to microcline Feldspar (001), J. Phys. Chem. Lett. **15**, 15 (2024).

[21] K. Kim, M. Abe, S. Kawai, and O. Custance, Exploring partially reduced CeO_2(111) surface at the atomic scale using scanning probe microscopy, Sci. Technol. Adv. Mater. **26**, 2528596 (2025).

[22] P. Wiesener, S. Förster, M. Merkel, B. S. Lammers, H. Fuchs, S. Amirjalayer, and H. Mönig, Standardization of chemically selective atomic force microscopy for metal oxide surfaces, ACS Nano **18**, 21948 (2024).

[23] L. Gross, B. Schuler, F. Mohn, N. Moll, N. Pavliček, W. Steurer, I. Scivetti, K. Kotsis, M. Persson, and G. Meyer, Investigating atomic contrast in atomic force microscopy and Kelvin probe force microscopy on ionic systems using functionalized tips, Phys. Rev. B **90**, 155455 (2014).

[24] M. Ellner, N. Pavliček, P. Pou, B. Schuler, N. Moll, G. Meyer, L. Gross, and R. Peréz, The electric field of CO tips and its relevance for atomic force microscopy, Nano Lett. **16**, 1974 (2016).

[25] R. Hoffmann, D. Weiner, A. Schirmeisen, and A. S. Foster, Sublattice identification in noncontact atomic force microscopy of the NaCl(001) surface, Phys. Rev. B **80**, 115426 (2009).

[26] A. J. Weymouth, M. Persson, and F. J. Giessibl, Revealing buckling of an apparently flat monolayer of NaCl on Pt(111), Phys. Rev. B **105**, 035412 (2022).

[27] K. Ruschmeier, A. Schirmeisen, and R. Hoffmann, Atomic-scale force-vector fields, Phys. Rev. Lett. **101**, 156102 (2008).

[28] A. Liebig, P. Hapala, A. J. Weymouth, and F. J. Giessibl, Quantifying the evolution of atomic interaction of a complex surface with a functionalized atomic force microscopy tip, Sci. Rep. **10**, 14104 (2020).

[29] M. Schneiderbauer, M. Emmrich, A. J. Weymouth, and F. J. Giessibl, CO tip functionalization inverts atomic force microscopy contrast via short-range electrostatic forces, Phys. Rev. Lett. **112**, 166102 (2014).

[30] G. Kresse and J. Furthmüller, Efficient iterative schemes for *ab initio* total-energy calculations using a plane-wave basis set., Phys. Rev. B **54**, 11169 (1996).

[31] G. Kresse and J. Furthmüller, Efficiency of *ab initio* total energy calculations for metals and semiconductors using a plane-wave basis set, Comput. Mater. Sci. **6**, 15 (1996).

[32] See Supplemental Material at http://link.aps.org/supplemental/10.1103/297b-7fpm for a more detailed description of the experimental setup, computational details and the probe particle simulations, which include Refs. [41–43].

[33] R. Bennewitz, V. Barwich, M. Bammerlin, C. Loppacher, M. Guggisberg, A. Baratoff, E. Meyer, and H.-J. Güntherodt, Ultrathin films of NaCl on Cu(111): A LEED and dynamic force microscopy study, Surf. Sci. **438**, 289 (1999).

[34] J. Repp, G. Meyer, and K.-H. Rieder, Snell's law for surface electrons: Refraction of an electron gas imaged in real space, Phys. Rev. Lett. **92**, 036803 (2004).

[35] F. Schulz, J. Ritala, O. Krejčí, A. P. Seitsonen, A. S. Foster, and P. Liljeroth, Elemental identification by combining atomic force microscopy and Kelvin probe force microscopy, ACS Nano **12**, 5274 (2018).

[36] R. Bolat, J. M. Guevara, P. Leinen, M. Knol, H. H. Arefi, M. Maiworm, R. Findeisen, R. Temirov, O. T. Hofmann, R. J. Maurer, F. S. Tautz, and C. Wagner, Electrostatic potentials of atomic nanostructures at metal surfaces quantified by scanning quantum dot microscopy, Nat. Commun. **15**, 2259 (2024).

[37] T. Esat, D. Borodin, J. Oh, A. J. Heinrich, F. S. Tautz, Y. Bae, and R. Temirov, A quantum sensor for atomic-scale electric and magnetic fields, Nat. Nanotechnol. **19**, 1466 (2024).

[38] R. Bennewitz, A. S. Foster, L. N. Kantorovich, M. Bammerlin, C. Loppacher, S. Schär, M. Guggisberg, E. Meyer, and A. L. Shluger, Atomically resolved edges and kinks of NaCl islands on Cu(111): Experiment and theory, Phys. Rev. B **62**, 2074 (2000).

[39] S. Mishra, M. Vilas-Varela, L.-A. Lieske, R. Ortiz, S. Fatayer, I. Rončević, F. Albrecht, T. Frederiksen, D. Peña, and L. Gross, Bistability between π-diradical open-shell and closed-shell states in indeno[1,2-*a*]fluorene, Nat. Chem. **16**, 755 (2024).

[40] P. Hapala, G. Kichin, C. Wagner, F. S. Tautz, R. Temirov, and P. Jelinek, Mechanism of high-resolution STM/AFM imaging with functionalized tips, Phys. Rev. B **90**, 085421 (2014).

[41] D. Yesilpinar, B. Schulze Lammers, A. Timmer, S. Amirjalayer, H. Fuchs, and H. Mönig, High resolution noncontact atomic force microscopy imaging with oxygen-terminated copper tips at 78 K, Nanoscale **12**, 2961 (2020).

[42] J. P. Perdew, K. Burke, and M. Ernzerhof, Generalized gradient approximation made simple., Phys. Rev. Lett. **77**, 3865 (1996).

[43] S. Grimme, S. Ehrlich, and L. Goerigk, Effect of the damping function in dispersion corrected density functional theory, J. Comput. Chem. **32**, 1456 (2011).